



Single Ligand Exchange on an Au-Cu Bimetal Nanocluster and Mechanism

Journal:	<i>Nanoscale</i>
Manuscript ID	NR-ART-02-2018-001611.R1
Article Type:	Paper
Date Submitted by the Author:	28-Apr-2018
Complete List of Authors:	Song, Yongbo; Anhui University, Lv, Ying; Anhui University, Department of Chemistry and Center for Atomic Engineering of Advanced Materials Zhou, Meng; Carnegie Mellon University, Chemistry Luo, Tian-Yi; University of Pittsburgh, Department of Chemistry Zhao, Shuo; Carnegie Mellon University Rosi, Nathaniel; University of Pittsburgh, Department of Chemistry Yu, Haizhu; Anhui University, Zhu, Manzhou; Anhui university, Department of Chemistry Jin, Rongchao; Carnegie Mellon University, Chemistry



Journal Name

ARTICLE

Single Ligand Exchange on an Au-Cu Bimetal Nanocluster and Mechanism

Yongbo Song,^{a,b} Ying Lv,^a Meng Zhou,^b Tian-Yi Luo,^c Shuo Zhao,^b Nathaniel L. Rosi,^c Haizhu Yu,^a Manzhou Zhu*^a, and Rongchao Jin*^b

Received 00th January 20xx,
Accepted 00th January 20xx

DOI: 10.1039/x0xx00000x

www.rsc.org/

An Au-Cu bimetallic nanocluster co-capped by selenolate and phosphine is obtained and its X-ray structure shows an icosahedral Au₁₃ kernel surrounded by three CuSe₂PPh₂Py motifs and one CuSe₃ motif, formulated as [Au₁₃Cu₄(PPh₂Py)₃(SePh)₉]. Interestingly, a *single-ligand-exchange* process is observed in the growth reaction, in which an [Au₁₃Cu₄(PPh₂Py)₄(SePh)₈]⁺ intermediate is first formed, but a prolong reaction leads to one PPh₂Py ligand being selectively replaced by a PhSe- ligand. DFT simulations reveal that both steric hindrance and bond dissociation energy have great effects on the single-ligand-exchange reaction as well as the thermodynamics, which helps to understand the mechanism of the ligand-exchange. Temperature-dependent UV-vis absorption and photoluminescence (PL) properties of the Au-Cu nanocluster imply that the optical properties are mainly contributed by the metal core. Femtosecond time-resolved pump-probe analysis maps out further details of the PL process.

Introduction

Recent years have witnessed significant advances in the research on metal nanoclusters with atomic precision.¹⁻³ Several strategies have been developed for precise synthetic control.⁴⁻¹¹ Among these methods, the ligand-exchange approach constitutes a recent development,⁷⁻¹¹ in which monodisperse nanoclusters are used as the precursors for etching by different ligands. With the ligand-exchange method,¹⁰ a series of new nanoclusters have been discovered, and many of them have been structurally determined owing to the high purity of the products made by the ligand exchange method, such as Au₂₀(SR)₁₆, Au₂₄(SR)₂₀, Au₂₈(SR)₂₀, Au₃₆(SR)₂₄, Au₁₃₃(SR)₅₂ and bimetal ones.¹²⁻¹⁸ These results have greatly enriched the diversity of metal nanoclusters.¹⁹

Beside its usefulness in preparing new metal nanoclusters with different size/structure, the ligand-exchange method has also helped to further understand the physicochemical properties of nanoclusters and broaden their applications.²⁰⁻³⁰ Ackerson's group reported ligand exchange on Au₁₀₂(SR)₄₄ and Au₂₅(SR)₁₈.^{20,21} Aikens and coworkers obtained mechanistic insights by theoretical simulations.²³ Xie and co-workers performed ligand-exchange on Au₂₅(SR)₁₈ to explore how the ligands affect the electronic structure

of the metal core.²⁵ Changing the ligands can also enhance the properties of metal nanoclusters; for instance, it has been reported that bulky ligands with strong conjugation effect can enhance the fluorescence of metal nanoclusters.^{26,27} New chiral properties can also be endowed to the metal nanocluster by exchanging with functionalized ligands,^{28,29} which will be beneficial to the application of metal nanoclusters in biomedicine and drug delivery.³⁰ Above all, the ligand-exchange method has shown vital impact on the development of metal nanoclusters.

Recently, there have been efforts to explore the mechanism of ligand-exchange.³¹⁻³⁴ Negishi and coworkers achieved high resolution isolation of ligand exchanged isomers.³¹ Jin and coworkers thoroughly investigated the transformation of Au₃₈ to Au₃₆ process by UV-vis absorption spectroscopy and ESI mass spectrometry.³² An unexpected disproportionation process was observed during the size and structure transformation.³² The kinetics of the conversion process, the steric hindrance and electronic conjugation effects of the ligand have also been investigated.^{3,31,32} But the general mechanism of ligand-exchange on nanoclusters is still not complete yet, because the ligand-exchange process is affected by many potential factors, such as the temperature, the amount of the added ligand, the concentration of solution, reaction time, ligand effects, and so on. Thus, it is still quite challenging to map out the clear mechanism of ligand-exchange and understand the mechanism. In previous work, Huo and co-workers achieved gold nanoparticles with a single surface functional ligand by ligand-exchange through a solid phase synthetic approach, and they also obtained gold nanoparticle-dendrimer conjugates using the monofunctional gold nanoparticles and dendrimer as reactants.^{35,36} The single-ligand-exchange process is also of particular interest to mechanism researchers, because it would help to clearly understand the initiation site on the

^a Department of Chemistry and Centre for Atomic Engineering of Advanced Materials, Anhui University, Hefei, Anhui 230601, P. R. China. E-mail: zmz@ahu.edu.cn

^b Department of Chemistry, Carnegie Mellon University, Pittsburgh, PA 15213, USA. E-mail: rongchao@andrew.cmu.edu

^c Department of Chemistry, University of Pittsburgh, Pittsburgh, PA 15260, USA. Electronic Supplementary Information (ESI) available: Detailed synthesis procedure, characterization, crystal structure refinements, computational details, and optical measurements, Fig. S1-S5, Table S1-S2, and CIF, see DOI: 10.1039/x0xx00000x

nanocluster surface²⁰ and determine the kinetic or thermodynamic factors of the ligand-exchange process. but single-ligand-exchange process on metal nanoclusters with exact structures has not been realized.^{3,20}

We have long been interested in preparing selenolate-protected metal nanoclusters and studying the ligand exchange mechanism.⁷ Recent work by Zheng and co-workers reported an $[\text{Au}_{13}\text{Cu}_4(\text{PPh}_2\text{Py})_4(\text{SPhBu}^t)_8]$ nanocluster co-protected by thiolate and phosphine.³⁷ Interestingly, there is one phosphine ligand in the Au-Cu nanocluster being different from other three phosphine ligands in terms of chemical environment.³⁷ We rationalize that this inequality may be utilized for inducing single-ligand-exchange using a suitable selenolate ligand. In our previous works^{26,38-40} we found that the selenolate ligands have several characteristics compared with the thiolate ligands for gold nanoclusters, including the selenolate's stronger bond energy, longer bond length and multi-coordinate mode.

In this work, an $\text{Au}_{13}\text{Cu}_4(\text{PPyPh}_2)_3(\text{SePh})_9$ nanocluster co-capped by selenolate and phosphine is successfully synthesized via single ligand exchange (i.e. $-\text{SePh}$ for PPh_2Py) on an $[\text{Au}_{13}\text{Cu}_4(\text{PPh}_2\text{Py})_4(\text{SPhBu}^t)_8]$ intermediate nanocluster during a one-pot growth process. The latter nanocluster is a selenolate counterpart of the $[\text{Au}_{13}\text{Cu}_4(\text{PPh}_2\text{Py})_4(\text{SPhBu}^t)_8]$ reported by Zheng et al.³⁷ The structure of the single-ligand-exchange product, $\text{Au}_{13}\text{Cu}_4(\text{PPyPh}_2)_3(\text{SePh})_9$, is determined by x-ray crystallography. DFT simulations are employed to understand the mechanism of single-ligand-exchange, which reveal that both steric hindrance and bond dissociation energy have significant effects on the single-ligand-exchange reaction. Furthermore, the optical properties (both absorption and luminescence) of this Au-Cu nanocluster are mainly contributed by the metal core.

Results and Discussion

Synthesis and characterization of the $\text{Au}_{13}\text{Cu}_4\text{Se}$ nanocluster

The $[\text{Au}_{13}\text{Cu}_4(\text{PPh}_2\text{Py})_3(\text{SePh})_9]$ ($\text{Au}_{13}\text{Cu}_4\text{Se}$ for short) nanocluster was synthesized by NaBH_4 reduction of mixed $\text{AuCl}(\text{PPh}_2\text{Py})$ and copper(II) acetylacetonate precursors. Polydisperse nanoclusters were first formed after NaBH_4 (aqueous) was added to the mixed metal precursors dissolved in dichloromethane. After 10 min, PhSeH was added to convert the polydisperse Au-Cu nanoclusters into monodisperse nanoclusters. After ~ 48 hours, the mixture in the organic phase was collected and washed several times with CH_3OH to remove the redundant PhSeH , PPh_2Py and by-products until the optical absorption spectrum showed two stepwise peaks at 375 (3.25eV) and 500 nm (2.47eV) (Fig. 1A). The as-obtained product was confirmed to be pure $\text{Au}_{13}\text{Cu}_4\text{Se}$ nanoclusters (*vide infra*). It is noteworthy that the yield of the nanocluster is very high ($> 90\%$, based on the metal atoms), demonstrating great potential of this strategy in batch synthesis. More details of the method are provided in the Supporting Information.

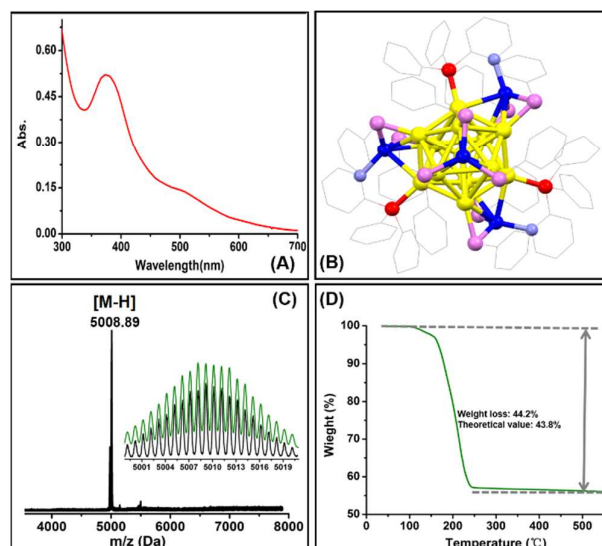


Fig. 1 (A) UV-vis absorption spectrum of the pure $\text{Au}_{13}\text{Cu}_4\text{Se}$ nanocluster; (B) Crystal structure; (C) ESI-MS analysis (inset: comparison of the experimental (black) and simulated (green) isotope patterns of the nanocluster); (D) thermogravimetric analysis of the nanocluster. Color labels: yellow = Au; blue = Cu; light blue = N; violet = Se; red = P; gray = C; the H atoms are all omitted for clarity.

Black cubic crystals of high quality were obtained by diffusion of ether into a dichloromethane solution of nanoclusters at room temperature (2-3 days). The dark crystals were analyzed by X-ray diffraction. The atomic structure of the nanocluster consists of an $\text{Au}_{13}\text{Cu}_4$ metal core protected by 3 Ph_2PyP -ligands and 9 PhSe -ligands (Fig. 1B), hence, formulated as $\text{Au}_{13}\text{Cu}_4(\text{PPyPh}_2)_3(\text{SePh})_9$. The product was also characterized by electrospray ionization mass spectrometry (ESI-MS) (Fig. 1C). The peak of high abundance is at m/z 5008.89, corresponding to $[\text{Au}_{13}\text{Cu}_4(\text{PPyPh}_2)_3(\text{SePh})_9]$ (theoretical value: 5010.15 Da). The observed isotope pattern is in good agreement with the simulated one according to the formula (Fig. 1C inset). The purity of the sample was further analyzed by thermogravimetric analysis (Fig. 1D), in which the observed loss of 44.2 wt% is consistent with the calculated 43.8 % according to the formula. All these results confirm the formula and the purity of the product.

Structural analysis of the $\text{Au}_{13}\text{Cu}_4\text{Se}$ nanocluster

The $\text{Au}_{13}\text{Cu}_4(\text{PPyPh}_2)_3(\text{SePh})_9$ nanocluster obtained in this work is interesting in consideration of its relationship with the previously reported $[\text{Au}_{13}\text{Cu}_4(\text{PPh}_2\text{Py})_4(\text{SPhBu}^t)_8]$ nanocluster³⁷ ($\text{Au}_{13}\text{Cu}_4\text{S}$ for short). Although the new $\text{Au}_{13}\text{Cu}_4\text{Se}$ shows a similar core structure as that of $\text{Au}_{13}\text{Cu}_4\text{S}$, distinct differences are found in the ligand shell. Compared with the previous $\text{Au}_{13}\text{Cu}_4\text{S}$ nanocluster, not only the eight RS-ligands are now replaced by PhSe -ligands, but also one PPh_2Py -ligand is replaced by one PhSe -ligand in the new $\text{Au}_{13}\text{Cu}_4\text{Se}$ nanocluster, hence, one "N-Cu-S₂" motif³⁷ is changed to a new "Cu-Se₃" motif. Interestingly, the motif change has significant effects on the symmetry of the $\text{Au}_{13}\text{Cu}_4\text{Se}$ nanocluster.

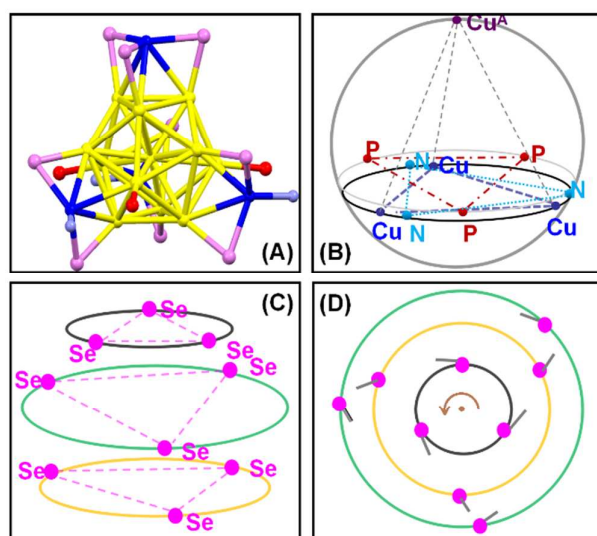


Fig. 2 Structural analysis of the $\text{Au}_{13}\text{Cu}_4\text{Se}$ nanocluster: the framework (A), the cartoon showing the arrangement of the Cu, N and P atoms (B), the Se atoms (C), and the benzene rings in PhSe-ligands (D).

For a detailed analysis of the arrangement of the Au, Cu, Se, and N atoms, the framework of the $\text{Au}_{13}\text{Cu}_4\text{Se}$ nanocluster is shown in Fig. 2A. The “N-Cu-Se₂” motif can be clearly seen (the Cu atoms are marked in blue). The length of Cu-Se in “N-Cu-Se₂” motifs is longer (average: 2.41 Å) than that of Cu-S in the “N-Cu-S₂” motifs (average: 2.28 Å), which is due to the larger radius of the Se atom (covalent radius of selenium atom $r = 1.20$ Å versus sulfur atom $r = 1.05$ Å).²⁶ Meanwhile, the angle of Se-Cu-Se is 122.37° in all “N-Cu-Se₂”, which is larger than the S-Cu-S angles³⁷ (103.32, 110.05 or 121.32°). Furthermore, the average Cu-Se length is 2.39 Å in the Cu-Se₃ motif, which is also longer than that of Cu-S but shorter than that of Cu-Se in the construction of N-Cu-Se₂ motifs.

Compared to the $\text{Au}_{13}\text{Cu}_4\text{S}$ counterpart,³⁷ the single ligand change (phosphine to selenolate) leads to high symmetry in the $\text{Au}_{13}\text{Cu}_4\text{Se}$ nanocluster, see schematic diagrams for the arrangements in the $\text{Au}_{13}\text{Cu}_4\text{Se}$ nanocluster (Fig. 2 B and 2C). As one can see in Fig. 2B, the Cu, N and P atoms form three equilateral triangles, respectively, and the corresponding lengths of sides are 7.445 Å, 10.018 Å and 8.596 Å, respectively (Fig. S1). Moreover, the triangular planes are parallel to each other. For comparison, the Se atoms in our structure can also be divided into three groups (Fig. 2C), and the Se atoms in each group can also form an equilateral triangle with the edge length of 4.140, 8.812, and 6.260 Å, respectively (Fig. S2). In addition to these, the Ph- in the selenolate ligand also abides by a rule: As shown in Fig. 2D (the gray bar represents the benzene ring), all the benzene rings are arranged in a counterclockwise direction, which is consistent with the direction of N-Cu bonds. All these results demonstrate that the single ligand-exchange from PPh_2Py to PhSe has induced the high symmetry.

Single-ligand-exchange from $[\text{Au}_{13}\text{Cu}_4(\text{PPh}_2\text{Py})_4(\text{SePh})_8]^+$ to $[\text{Au}_{13}\text{Cu}_4(\text{PPh}_2\text{Py})_3(\text{SePh})_9]$

According to the results and analysis above, an interesting question is whether $[\text{Au}_{13}\text{Cu}_4(\text{PPh}_2\text{Py})_4(\text{SePh})_8]^+$ (the selenolate counterpart of the $\text{Au}_{13}\text{Cu}_4\text{S}$ nanocluster) would exist in our synthetic process.

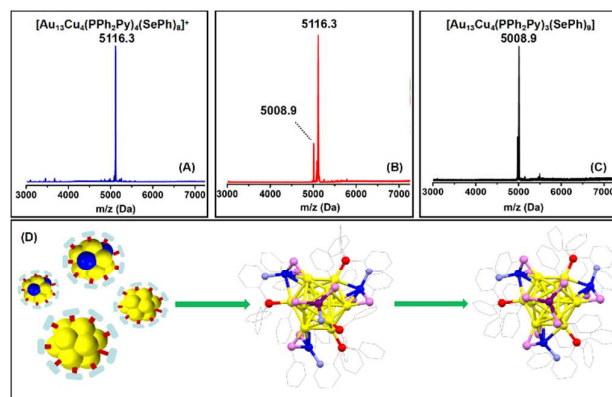


Fig. 3 The growth process of the $\text{Au}_{13}\text{Cu}_4\text{Se}$ nanocluster: the ESI mass spectra of the product at 8 h (A), 14 h (B), and 48 h (C), and the growth mechanism (D).

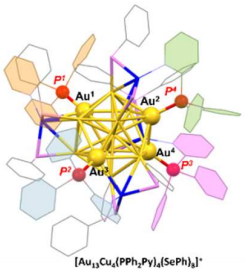
To investigate this, we used mass spectrometry to monitor the reaction process. All the ESI mass spectra were obtained under the positive mode (without adding Cs^+). Interestingly, at 8 h of the growth process, the mass spectrum shows a peak at 5116.3 Da (Fig. 3A), which is assigned to $[\text{Au}_{13}\text{Cu}_4(\text{PPh}_2\text{Py})_4(\text{SePh})_8]^+$ (cal. 5116.28 Da), and the observed isotope pattern is in agreement with the simulated one according to the formula (Fig. S3). The result indicates that $[\text{Au}_{13}\text{Cu}_4(\text{PPh}_2\text{Py})_4(\text{SePh})_8]^+$ exists as an early stage product during the reaction. After a prolonged reaction time (14h, Fig. 3B), a new peak at 5008.9 Da was simultaneously observed, which corresponds to the $[\text{Au}_{13}\text{Cu}_4(\text{PPh}_2\text{Py})_3(\text{SePh})_9]$ nanocluster (cal. 5010.15 Da); of note, here one PPh_2Py ligand is already replaced by one -SePh ligand. Further extension of the reaction time leads to a sole peak at 5008.9 Da as the final product (Fig. 3C), which indicates that the intermediate $[\text{Au}_{13}\text{Cu}_4(\text{PPh}_2\text{Py})_4(\text{SePh})_8]^+$ nanoclusters have been completely converted to the $\text{Au}_{13}\text{Cu}_4(\text{PPh}_2\text{Py})_3(\text{SePh})_9$ nanoclusters.

According to the above mass spectrometry results, the formation process of the $\text{Au}_{13}\text{Cu}_4\text{Se}$ is shown in Fig. 3D. After the reduction of the phosphine-capped Au/Cu complexes, a polydisperse Au-Cu product was first produced (Fig. 3D, left), which is then converted into monodisperse $[\text{Au}_{13}\text{Cu}_4(\text{PPh}_2\text{Py})_4(\text{SePh})_8]^+$ nanoclusters (Fig. 3D, middle) in the presence of PSeH and PPh_2Py . Finally, one PPh_2Py -ligand is replaced by one PhSe- ligand, and $\text{Au}_{13}\text{Cu}_4(\text{PPh}_2\text{Py})_3(\text{SePh})_9$ nanoclusters are generated as the final product (Fig. 3D, right). Such a single-ligand exchange process is quite remarkable. It is also worth noting that, before/after single-ligand-exchange, both Au-Cu nanoclusters follow the 8e count ($8 = 13 + 4 - 8 - 1$, or $8 = 13 + 4 - 9$).

Density functional theory (DFT) analysis

The above results clearly show that $[\text{Au}_{13}\text{Cu}_4(\text{PPh}_2\text{Py})_3(\text{SePh})_9]$ grows from the $[\text{Au}_{13}\text{Cu}_4(\text{PPh}_2\text{Py})_4(\text{SePh})_8]^+$ nanocluster through single ligand exchange. Some interesting questions arise: 1) Why the PhSe-ligand preferentially replaces one of the four PPh_2Py -ligands? 2) Considering the similar Au-P bonds, what is the driving force to promote the selective substitution. To answer these questions and obtain insight into the single ligand exchange mechanism, density functional theory (DFT) calculations are carried out.⁴¹

Table 1. Density functional theory calculations on the key parameters of the $[\text{Au}_{13}\text{Cu}_4(\text{PPh}_2\text{Py})_3(\text{SePh})_8]^+$ nanocluster.

	n	1	2	3	4
	Bond distance of $\text{Au}^n\text{-P}^n$ (Å)	2.338	2.339	2.339	2.344
	BDE($\text{Au}^n\text{-P}^n$) (eV)	2.73	2.64	2.60	2.43
	Mulliken charge on P^n (e)	0.462	0.454	0.451	0.423

We constructed the initial structure of $[\text{Au}_{13}\text{Cu}_4(\text{PPh}_2\text{Py})_4(\text{SePh})_8]^+$ from the thiolate counterpart, $[\text{Au}_{13}\text{Cu}_4(\text{PPh}_2\text{Py})_4(\text{SR})_8]^+$ reported by Zheng et al.,³⁷ by replacing the S atoms with Se ones. The initial configuration of $[\text{Au}_{13}\text{Cu}_4(\text{PPh}_2\text{Py})_3(\text{SePh})_9]$ was taken from the crystal structure solved in the current work. The replacement of PPh₂Py-ligands at different locations by PhSe-ligands was first simulated. The geometry optimization in gas phase was carried out on both structures to locate the local minimum.⁴²⁻⁴³ For clarity, the four phosphine ligands were designated as P^1 , P^2 , P^3 , P^4 (Table 1), respectively. P^4 corresponded to the exchanged phosphine ligand by selenol observed experimentally. According to the calculation results (Table 1), all the four Au-P bond lengths in $[\text{Au}_{13}\text{Cu}_4(\text{PPh}_2\text{Py})_4(\text{SePh})_8]^+$ nanocluster are very similar, whereas the $\text{Au}^4\text{-P}^4$ bond distance (2.344 Å) is slightly longer than other ones (2.338, 2.339 and 2.339 Å).

The relatively longer $\text{Au}^4\text{-P}^4$ bond might be caused by the higher steric hindrance herein. Meanwhile, from the electronic effect, the Mulliken charge analysis⁴⁴ indicates that all the four PR_3 ligands (P^1 , P^2 , P^3 , P^4 , see Table 1) in the $[\text{Au}_{13}\text{Cu}_4(\text{PPh}_2\text{Py})_4(\text{SePh})_8]^+$ nanocluster are positively charged (i.e., 0.462, 0.454, 0.451 and 0.423). These data are expected, because the phosphine ligands act as electron-donors in the nanocluster. Nevertheless, P^4 carries the least positive charge (0.423) and thus exhibits the weakest electron-donating ability. In other words, the interaction between P^4 ligand and the metal core of $[\text{Au}_{13}\text{Cu}_4(\text{PPh}_2\text{Py})_4(\text{SePh})_8]^+$ nanocluster is relatively weaker than all the other phosphine ligands. Therefore, both the steric and electronic effects indicate that $\text{Au}^4\text{-P}^4$ bond is the most labile one, which would be preferentially attacked in the ligand-exchange reaction. Due to these reasons, the dissociation of the P^4 ligand is easier than all the other phosphine ligands, with the bond dissociation energy (BDE,⁴⁵ an illustrative diagram is given in Fig. S4) of $\text{Au}^n\text{-P}^n$ ($n=1-4$) being 2.73 eV, 2.64 eV, 2.60 eV, and 2.43 eV, respectively (Table 1). The weaker $\text{Au}^4\text{-P}^4$ bond results in the easier replacement of P^4 by PhSeH. Therefore, the calculation results corroborate and explain the preferential replacement of P^4 over other phosphine ligands. Note that in our calculations, the solvent effect on the concerned $\text{Au}\text{-P}^n$ interactions is also examined using COSMO⁴⁶⁻⁴⁸ solvent models. CH_2Cl_2 is chosen as the solvent (the one used in our experiments). Similar to the gas-phase calculations, the calculation results with solvent models (Table S1) also show that the $\text{Au}^4\text{-P}^4$ interaction is the weakest among different $\text{Au}^n\text{-P}^n$. Meanwhile, the formation of $[\text{Au}_{13}\text{Cu}_4(\text{PPh}_2\text{Py})_3(\text{SePh})_9]$ nanocluster

via exchanging a single phosphine ligand on $[\text{Au}_{13}\text{Cu}_4(\text{PPh}_2\text{Py})_4(\text{SePh})_8]^+$ nanocluster with phenylselenolate is also thermodynamically favored by 3.17 eV (Fig. S5).

While the computational results clearly show the preferential replacement of P^4 by selenol, these results do not demonstrate the kinetic features of the ligand exchange process. For this process, both dissociative (phosphine dissociation with subsequent selenol coordination) and associative (synergistic phosphine dissociation and selenol coordination) mechanisms are plausible. However, due to the strong Au-P bond strength (with BDE over 2 eV), the dissociative is suggested to be unlikely, and therefore the associative mechanism is more reasonable and proved. Of note, the associative selenol-for-phosphine mechanism also correlates with the thiol-for-thiol exchange mechanism reported recently.^{49,50}

Optical absorption and luminescence properties

The $\text{Au}_{13}\text{Cu}_4\text{Se}$ nanocluster exhibits moderately strong photoluminescence (PL) centered at 750 nm (QY=2-3%) (Fig. 4A), which is similar to the case of Au_{13} nanoclusters (QY=5%).⁵¹ Because the emission spectra show no dependence on the excitation wavelength (Fig. 4A), all the emissions should originate from the same (lowest) excited state. The PL excitation spectrum monitored at 750 nm emission shows peaks at 380 nm, 500 nm and 605 nm, which agree well with the absorption peaks; indeed, both the excitation and absorption spectra share a similar profile (Fig. 4A). As the absorption spectrum is mainly contributed by the metal core, the similar spectra of PLE and UV-vis absorption suggest that the PL is also mainly contributed by the metal core.

To elucidate the role of phonons (i.e. ionic lattice vibrations) in the PL of $\text{Au}_{13}\text{Cu}_4\text{Se}$ nanoclusters, temperature dependent UV-vis absorption and PL spectra were measured between 300 K and 80 K (Fig. 4B and C). As the temperature decreases, the absorption peaks become stronger and sharpened. Moreover, at low temperatures, the 380 nm absorption is split into 360 nm (main peak) and 390 nm (a shoulder); meanwhile, an additional peak at ~475 nm emerges next to the 500 nm peak. Interestingly, there is no significant peak shift at low temperatures (Fig. 4B), which is in contrast to the case of $\text{Au}_{25}(\text{SR})_{18}$ nanoclusters reported by Devadas et al.⁵² In low temperature PL measurements, one can observe that, as the temperature drops from 300 K to 80 K, the PL is enhanced by 6.6 times (calculated by the peak area), while the spectral profile remains almost the same (Fig. 4C). Only a slight redshift of the PL peak from 750 nm to 760 nm was observed.

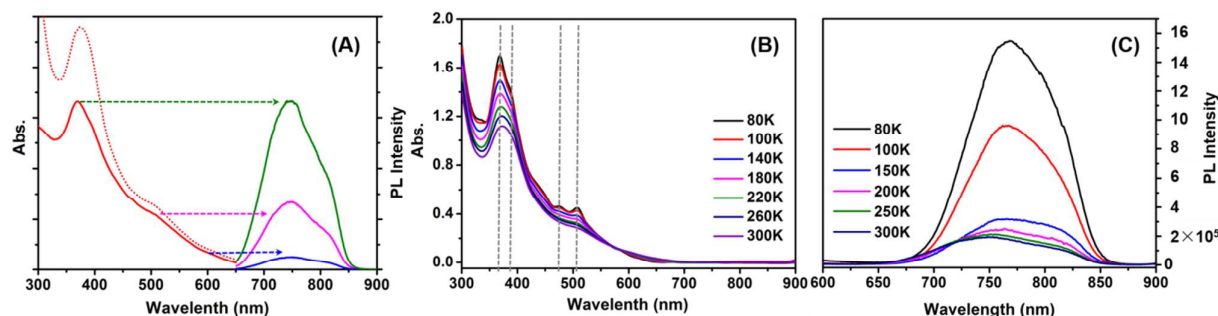


Fig. 4 Optical properties of Au₁₃Cu₄Se nanoclusters. (A) PL excitation spectrum (left, solid line) and emission spectra (right, solid lines), absorption spectrum (dashed line) was also shown for comparison; (B) UV-vis absorption spectra as a function of temperature; (C) PL emission spectra as a function of temperature.

Femtosecond time-resolved pump-probe experiment was further performed on Au₁₃Cu₄Se nanoclusters to probe its excited state dynamics (Fig. 5). Similar to other sized gold nanoclusters, broad excited state absorption (ESA, positive signals) are overlapped with ground state bleaching (GSB, negative signals) at around 500 nm and 600 nm (Fig. 5A). In the first 1 ps, ultrafast internal conversion (~ 270 fs) was observed (Fig. 5A and B), which is similar to the case of Au₁₃ nanoclusters.⁵³ Upon excitation, the GSB was initially at ~ 540 nm between 1 ps and 10 ps but gradually blueshifted to 510 nm (Fig. 5A, C and D), which was also reflected in the kinetic traces (Figure 5B). Such a phenomenon was not observed in the Au₁₃ nanoclusters.⁵³ In Au₂₅(SR)₁₈ nanoclusters, a blueshift of GSB was also observed in the TA spectra, which was assigned to the overlapped ESA decay. Here, the steady state absorption peak is at ~ 510 nm, which corresponds to the final GSB position. Therefore, decaying of ESA at around the same region (510 nm) should explain the blueshift of GSB. We attribute the additional 2 ps decaying component in Au₁₃Cu₄Se nanocluster (no similar decay in the Au₁₃ nanocluster⁵³) to a new non-radiative decay, which also explains the lower PL QY of Au₁₃Cu₄Se than Au₁₃.

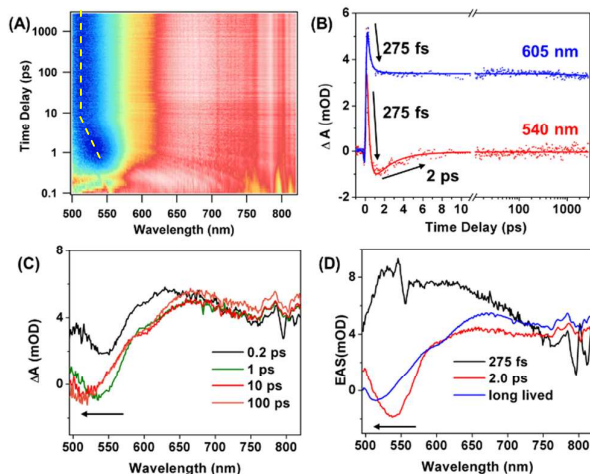


Fig. 5 Transient absorption spectroscopy of Au₁₃Cu₄Se nanoclusters with optical excitation at 490 nm. (A) Transient absorption data map of Au₁₃Cu₄Se with excitation of 490 nm, red color indicates positive signal while blue color indicates negative signal; (B) Kinetic traces and fitting at selected wavelengths; (C) TA spectra at different time delays. (D) Evolution associated spectra (EAS) obtained from global analysis.

Conclusion

In this work, an Au-Cu bimetallic nanocluster co-protected by selenolate and phosphine with a formula of [Au₁₃Cu₄(PPh₂Py)₃(SePh)₉] is successfully synthesized, and its structure shows an Au₁₃ core surrounded by three N-Cu-Se₂ motifs and a Cu-Se₃ motif. Compared with the [Au₁₃Cu₄(PPh₂Py)₄(SR)₈]⁺ nanocluster reported previously, the single ligand exchange from phosphine to selenolate greatly enhances the symmetry of the Au₁₃Cu₄Se nanocluster. More importantly, the single ligand exchange process was observed during the growth of Au₁₃Cu₄Se nanoclusters. Theoretical results demonstrate that both steric hindrance and bond dissociation energy play a critical role in the single ligand-exchange reaction, which offers insight into the mechanism of ligand-exchange. Furthermore, femtosecond time-resolved pump-probe experiment illustrates the lower PL QY in Au₁₃Cu₄Se nanoclusters compared with that of phosphine-capped Au₁₃ nanoclusters. Achieving single ligand exchange will provide potential opportunities for mono-functionalization of such nanoclusters for site-specific probing and sensing applications in future work.

Conflicts of interest

There are no conflicts to declare.

Acknowledgements

M.Z. acknowledges financial support by NSFC (21372006, U1532141, 21631001), the Ministry of Education, the Education Department of Anhui Province, 211 Project of Anhui University. R.J. acknowledges the Air Force Office of Scientific Research under AFOSR Award No. FA9550-15-1-9999 (FA9550-15-1-0154) and DURIP (FA9550-16-1-0218).

References

- 1 R. Jin, *Nanoscale* 2015, **7**, 1549.
- 2 P. Maity, S. Xie, M. Yamauchi, and T. Tsukuda, *Nanoscale* 2012, **4**, 4027.

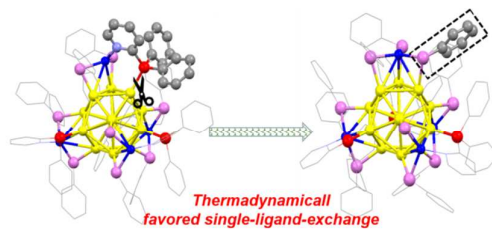
- 3 Y. Niihori, S. Hossain, S. Sharma, B. Kumar, W. Kurashige and Y. Negishi, *Chem. Rec.* 2017, **17**, 473.
- 4 Z. Wu, J. Suhan, and R. Jin, *J. Mater. Chem.* 2009, **19**, 622.
- 5 L. Liao, C. Yao, C. Wang, S. Tian, J. Chen, M.-B. Li, N. Xia, N. Yan and Z. Wu, *Anal. Chem.* 2016, **88**, 11297.
- 6 R. Jin, H. Qian, Z. Wu, Y. Zhu, M. Zhu, A. Mohanty, and N. Garg, *J. Phys. Chem. Lett.* 2010, **1**, 2903.
- 7 X. Meng, Q. Xu, S. Wang, and M. Zhu, *Nanoscale* 2012, **4**, 4161.
- 8 L. G. AbdulHalim, N. Kothalawala, L. Sinatra, A. Dass, and O. M. Bakr, *J. Am. Chem. Soc.* 2014, **136**, 15865.
- 9 Y. Niihori, M. Matsuzaki, T. Pradeep, and Y. Negishi, *J. Am. Chem. Soc.* 2013, **135**, 4946.
- 10 C. Zeng, Y. Chen, A. Das, and R. Jin, *J. Phys. Chem. Lett.* 2015, **6**, 2976.
- 11 E. Khatun, A. Ghosh, D. Ghosh, P. Chakraborty, A. Nag, B. Mondal, S. Chennu, and T. Pradeep, *Nanoscale* 2017, **9**, 8240.
- 12 C. Zeng, T. Li, A. Das, N. L. Rosi, and R. Jin, *J. Am. Chem. Soc.* 2013, **135**, 10011.
- 13 C. Zeng, H. Qian, T. Li, G. Li, N. L. Rosi, B. Yoon, R. N. Barnett, R. L. Whetten, U. Landman, and R. Jin, *Angew. Chem. Int. Ed.* 2012, **51**, 13114.
- 14 C. Zeng, C. Liu, Y. Chen, N. L. Rosi, and R. Jin, *J. Am. Chem. Soc.* 2014, **136**, 11922.
- 15 C. Zeng, Y. Chen, K. Kirschbaum, K. Appavoo, M. Y. Sfeir, and R. Jin, *Sci. Adv.* 2015, **1**, e1500045.
- 16 A. Dass, S. Theivendran, P. R. Nimmala, C. Kumara, V. R. Jupally, A. Fortunelli, L. Sementa, G. Barcaro, X. Zuo, and B. C. Noll, *J. Am. Chem. Soc.* 2015, **137**, 4610.
- 17 A. Das, T. Li, G. Li, K. Nobusada, C. Zeng, N. L. Rosi, and R. Jin, *Nanoscale* 2014, **6**, 6458.
- 18 M. S. Bootharaju, S. M. Kozlov, Z. Cao, M. Harb, M. R. Parida, M. N. Hedhili, O. F. Mohammed, O. M. Bakr, L. Cavallo and J. M. Basset, *Nanoscale* 2017, **9**, 9529.
- 19 R. Jin, C. Zeng, M. Zhou, and Y. Chen, *Chem. Rev.* 2016, **116**, 10346.
- 20 C. L. Heinecke, T. W. Ni, S. Malola, V. Mäkinen, O. A. Wong, H. Häkkinen and C. J. Ackerson, *J. Am. Chem. Soc.* 2012, **134**, 13316.
- 21 T. W. Ni, M. A. Tofanelli, B. D. Phillips and C. J. Ackerson, *Inorg. Chem.* 2014, **53**, 6500.
- 22 A. Fernando and C. M. Aikens, *J. Phys. Chem. C* 2016, **120**, 14948.
- 23 A. C. Templeton, W. P. Wuelfing, and R. W. Murray, *Acc. Chem. Res.* 2000, **33**, 27.
- 24 M. Lucarini, and L. Pasquato, *Nanoscale* 2010, **2**, 668
- 25 X. Yuan, N. Goswami, W. Chen, Q. Yao, and J. Xie, *Chem. Commun.* 2016, **52**, 5234.
- 26 Y. Song, J. Zhong, S. Yang, S. Wang, T. Cao, J. Zhang, P. Li, D. Hu, Y. Pei, and M. Zhu, *Nanoscale* 2014, **6**, 13977.
- 27 S. Wang, X. Zhu, T. Cao, and M. Zhu, *Nanoscale* 2014, **6**, 5777.
- 28 S. Knoppe, R. Azoulay, A. Dass, and T. Bürgi, *J. Am. Chem. Soc.* 2012, **134**, 20302.
- 29 M. Zhu, H. Qian, X. Meng, S. Jin, Z. Wu, and R. Jin, *Nano Lett.* 2011, **11**, 3963.
- 30 N. L. Rosi, D. A. Giljohann, C. S. Thaxton, A. K. R. Lytton-Jean, M. S. Han, and C. Mirkin, *Science* 2006, **312**, 1027.
- 31 Y. Niihori, Y. Kikuchi, A. Kato, M. Matsuzaki and Y. Negishi, *ACS Nano* 2015, **9**, 9347.
- 32 C. Zeng, C. Liu, Y. Pei, and R. Jin, *ACS Nano* 2013, **7**, 6138.
- 33 P. R. Nimmala, and A. Dass, *J. Am. Chem. Soc.* 2014, **136**, 17016.
- 34 S. Hossain, W. Kurashige, S. Wakayama, B. Kumar, L. V. Nair, Y. Niihori, and Y. Negishi, *J. Phys. Chem. C* 2016, **120**, 25861.
- 35 J. G. Worden, A. W. Shaffer and Q. Huo, *Chem. Commun.* 2004, 518.
- 36 J. G. Worden, Q. Dai and Q. Huo, *Chem. Commun.* 2006, 1536.
- 37 H. Yang, Y. Wang, J. Lei, L. Shi, X. Wu, V. Mäkinen, S. Lin, Z. Tang, J. He, H. Häkkinen, L. Zheng, and N. Zheng, *J. Am. Chem. Soc.* 2013, **135**, 9568.
- 38 Y. Song, S. Jin, X. Kang, J. Xiang, H. Deng, H. Yu, and M. Zhu, *Chem. Mater.* 2016, **28**, 2609.
- 39 Y. Song, S. Wang, J. Zhang, X. Kang, S. Chen, P. Li, H. Sheng, and M. Zhu, *J. Am. Chem. Soc.* 2014, **136**, 2963.
- 40 Y. Song, F. Fu, J. Zhang, J. Chai, X. Kang, P. Li, S. Li, H. Zhou, M. Zhu, *Angew. Chem. Int. Ed.* 2015, **54**, 8430.
- 41 G. Velde, F. M. Bickelhaupt, E. J. Baerends, C. F. Guerra, S. J. A. Gisbergen, J. G. Snijders, and T. Ziegler, *J. Comput. Chem.* 2001, **22**, 931.
- 42 J. P. Perdew, K. Burke, and M. Ernzerhof, *Phys. Rev. Lett.* 1996, **77**, 3865.
- 43 K. A. Kacprzak, L. Lehtovaara, J. Akola, O. Lopez-Acevedo, and H. Häkkinen, *Phys. Chem. Chem. Phys.* 2009, **11**, 7123.
- 44 R. S. Mulliken, *J. Chem. Phys.* 1955, **23**, 1833.
- 45 $BDE(Au^n-P^m) = E([Au_{13}Cu_4(PPh_2Py)_3(SePh)_8]^+) + E(P^m) - E[Au_{13}Cu_4(PPh_2Py)_4(SePh)_8]^+$. $E[Au_{13}Cu_4(PPh_2Py)_4(SePh)_8]^+$ is the energy of $[Au_{13}Cu_4(PPh_2Py)_4(SePh)_8]^+$ generated by geometry optimization, while $E([Au_{13}Cu_4(PPh_2Py)_3(SePh)_8]^+)$, $E(P^m)$ corresponds to single point energy of the two structural motifs after Au^n-P^m bond dissociation.
- 46 A. Klamt and G. Schüürmann, *J. Chem. Soc.: Perkin Trans.* 1993, **2**, 799.
- 47 A. Klamt, *J. Phys. Chem.* 1995, **99**, 2224.
- 48 A. Klamt and V. Jones, *J. Chem. Phys.* 1996, **105**, 9972.
- 49 C. Zeng, Y. Chen, A. Das, and R. Jin, *J. Phys. Chem. Lett.* 2015, **6**, 2976.
- 50 M. J. Hostetler, A. C. Templeton, and R. W. Murray, *Langmuir* 1999, **15**, 3782.
- 51 Y. Shichibu, and K. Konishi, *Small* 2010, **6**, 1216.
- 52 M. S. Devadas, S. Bairu, H. Qian, E. Sinn, R. Jin, and G. Ramakrishna, *J. Phys. Chem. Lett.* 2011, **2**, 2752.
- 53 M. Zhou, R. Jin, M. Y. Sfeir, Y. Chen, Y. Song, and R. Jin, *PNAS* 2017, **114**, 4697.



Journal Name

ARTICLE

TOC:



Single-ligand-exchange between phosphine and selenolate on $\text{Au}_{13}\text{Cu}_4$ is achieved and the process exhibits high site-specificity.